INSTITUTE OF PHYSICS PUBLISHING JOURNAL OF PHYSICS D: APPLIED PHYSICS

J. Phys. D: Appl. Phys. **34** (2001) A82–A86 www.iop.org/Journals/jd PII: S0022-3727(01)21444-2

Double-crystal x-ray diffractometry of single crystals with microdefects

V B Molodkin[1], S I Olikhovskii[1], E N Kislovskii[1], V P Krivitsky[1], E G Len'[1], E V Pervak[1], G E Ice[2] and B C Larson[2]

[1] G.V.Kurdyumov Institute for Metal Physics, NAS of Ukraine, 36, Vernadsky blvd, Kyiv-142, UA-03680, Ukraine
[2] Oak Ridge National Laboratory, Oak Ridge, TN 37831-6118, USA

E-mail: tatar@imp.kiev.ua (V B Molodkin)

Received 13 September 2000

Abstract
The known method of the 'integral' diffuse scattering has been generalized in the Bragg case of x-ray diffraction for crystals, which contain large microdefects commensurable with the extinction length. In the framework of the developed statistical dynamical theory, relatively simple analytical expressions have been derived for coherent and diffuse components of reflectivity of single crystals with randomly distributed microdefects.

To test the characterization possibilities of the proposed method, the rocking curves (RCs) of Czochralski-grown silicon single crystal annealed at 1080 °C for 6 h have been measured for 111 and 333 reflections of Cu $K_{\alpha 1}$ radiation using a high-resolution double-crystal x-ray diffractometer. The fitting results for the two RCs are in good mutual agreement and demonstrate the high information ability of the method.

1. Introduction

The method of integral diffuse scattering (DS) of x-rays, proposed by Dederichs [1, 2] and developed by Larson [3, 4], is widely used to characterize the point defects and their clusters in various crystalline materials. The method makes use of the angular dependences of the DS intensity integrated over exit angles. These dependences are measured by double-crystal diffractometer (DCD) far from the Bragg peak and are treated using the formulae derived for various type defects from the known expressions of the kinematical theory for the differential DS intensity [1, 5]. The application efficiency of the method is provided by the high sensitivity of these dependences to defect sizes.

However, in the investigation of microdefects in silicon [6–8] this method meets with some difficulties. Firstly, the measurable DS intensity distributions are very close to the Bragg peak because of large effective sizes of the microdefects. In such cases, the correct interpretation of the measured angular distributions of x-ray scattering intensity must account for the dynamical DS effects in this region and for the contribution of the coherent component. Secondly, it is necessary to account for the simultaneous presence of several types of microdefects in the silicon crystal (oxygen precipitates, dislocation loops, stacking faults, etc [9]).

These difficulties can be overcome by using the generalized dynamical theory of x-ray scattering by single crystals containing homogeneously distributed defects [10, 11]. This theory has been extended in [12] for the case of single crystals with microdefects, which have large effective radii commensurable with the extinction length. Here, the analytical expressions derived in [12] for the coherent and diffuse components of reflection power of such crystals will be applied to characterize the defects in the annealed silicon single crystal by using the RCs measured by the high-resolution DCD with widely open detector window.

The theoretical bases and formulae used are elucidated in section 2. X-ray optic schemes of the measurements and the investigated silicon sample are described in section 3. The procedure of the treatment of measured RCs is explained and the obtained results are discussed in section 4.

2. Reflection coefficient of imperfect single crystal

The coherent scattering of x-rays by the periodical part of the crystal potential in imperfect single crystals containing randomly distributed microdefects is accompanied by elastic DS on the fluctuations of static displacement fields of matrix atoms. The influence of DS on the amplitudes of coherent waves rises significantly with increasing defect sizes. The enlarged defect radii also cause a concentration of DS intensity in the close vicinity of reciprocal lattice points, i.e. near the directions exactly satisfying the Bragg condition, and therefore

an account of the dynamical effects in DS becomes necessary for the detailed quantitative description of diffraction patterns.

The amplitudes of the strong Bragg (coherent) waves in a crystal with chaotically distributed microdefects satisfy the same homogeneous set of algebraic equations as in the perfect crystal [13], but with the coefficients including the modified Fourier components of the crystal polarizability [10–12]. The modification consists of multiplying the Fourier components of perfect crystal polarizability $\chi_{\pm \boldsymbol{H}}$ by the static Debye–Waller factor $E = \exp(-L_{\boldsymbol{H}})$, where $\boldsymbol{H}$ is 2π times the reciprocal lattice vector corresponding to the considered Bragg reflection, and adding to this term, and to χ_0, the so-called dispersion corrections arising due to the elastic scattering of coherent waves into diffuse ones. For the two-beam case of x-ray diffraction, this basic equation set can be solved easily, and, after substitution of the found wave amplitudes into the usual boundary conditions for the Bragg case of x-ray diffraction by the parallel-sided crystal plate, one can calculate the amplitude $E^a_{\boldsymbol{H}}$ of the diffracted plane wave in vacuum.

When the approximation of the semi-infinite crystal is valid, i.e. the inequality $\mu_0 t \gg 1$ holds, where μ_0 is the linear coefficient of photoelectric absorption and t is the crystal thickness, only one wave field remains in the crystal. Then, the expression for $E^a_{\boldsymbol{H}}$ is simplified, and the coherent component of reflection coefficient can be calculated by the known formula for perfect crystal [13] but with some modification [12]:

$$R_{coh}(\Delta\theta) = \frac{|\gamma_H||E^a_{\boldsymbol{H}}|^2}{\gamma_0|E_0|^2} = \varsigma(L - \sqrt{L^2 - 1}) \qquad (1)$$

with

$$L = [z^2 + (g+h)^2 + \{[z^2 - (g+h)^2 - E^2(1-\kappa^2-a^2)]^2 + 4[z(g+h) - E^2(p+d)]^2\}^{1/2}] \times \left[E^2\sqrt{(1-\kappa^2-a^2)^2 + 4(p+d)^2}\,\right]^{-1}$$

$$z = \frac{\Delta\theta \sin(2\theta_B)}{C|\chi_{r\boldsymbol{H}}|}\sqrt{b} \qquad b = \frac{\gamma_0}{|\gamma_H|}.$$

Here, E_0 is the incident plane wave amplitude, γ_0 and γ_H are direction cosines of incident and diffracted x-rays respectively, $\zeta \approx 1$, $\Delta\theta$ is rocking angle, θ_B is Bragg angle, $C = 1$ or $\cos(2\theta_B)$ is the polarization factor, $\chi_{r\boldsymbol{H}}$ is the Fourier component of the real part of crystal polarizability and the parameters g, κ and p account for the absorption due to the inelastic scattering processes (photoelectric absorption, Compton scattering and thermal diffuse scattering) and are the same as in perfect crystal [13]. Parameters h, d and a take account of the additional effective absorption of the strong Bragg waves due to the elastic DS caused by defects. The joint influence of the static Debye–Waller factor and the additional absorption parameters leads to the narrowing and decreasing of the coherent component of the reflection coefficient as compared to that of perfect crystal.

Diffusely scattered waves are created due to the scattering of the strong Bragg waves by the fluctuation field of the static displacements of crystal atoms, which are caused by chaotically distributed defects, and also form in crystal the dynamical wave field. In the two-beam case of diffraction, the amplitudes of two diffusely scattered plane waves forming the diffuse quasi-Bloch wave satisfy the set of inhomogeneous equations which describe the multiple rescattering processes of diffuse waves on the periodical part of the crystal potential as well as the multiple processes of diffuse scattering from the strong Bragg and diffusely scattered waves into the diffuse ones.

Imposing the boundary conditions on the diffuse wave amplitudes for the Bragg case of diffraction and transforming the derived plane wave amplitudes at the crystal surface into the scattering amplitude $f_{\boldsymbol{H}}(\boldsymbol{K}', \boldsymbol{K})$ and the corresponding differential cross section $\mathrm{d}\sigma/\mathrm{d}\Omega_{\boldsymbol{K}'}$ of the DS into the solid angle in the direction $\boldsymbol{K}'$, one can obtain the diffuse component of the differential reflection power of the crystal ($\delta = 1, 2$; $\boldsymbol{G} = 0, \boldsymbol{H}$):

$$R_{DS}(\boldsymbol{k}) = \frac{\langle |f_{\boldsymbol{H}}(\boldsymbol{K}', \boldsymbol{K})|^2\rangle}{\gamma_0 S|E_0|^2} \qquad (2)$$

$$f_{\boldsymbol{H}}(\boldsymbol{K}', \boldsymbol{K}) = \sum_{\delta}\sum_{\boldsymbol{G}} D^{\delta}_{\boldsymbol{G}}(\boldsymbol{K}) F^{\delta}_{\boldsymbol{HG}}(\boldsymbol{K}', \boldsymbol{K}) \qquad (3)$$

where the corner brackets denote the averaging over a random distribution of defects, S is the entrance surface area, $D^{\delta}_{\boldsymbol{G}}(\boldsymbol{K})$ are amplitudes of strong Bragg waves, $F^{\delta}_{\boldsymbol{HG}}(\boldsymbol{K}', \boldsymbol{K})$ are the partial amplitudes of the scattering of strong Bragg waves into the diffuse ones, the vector $\boldsymbol{k} = \boldsymbol{K}' - \boldsymbol{K} - \boldsymbol{H}$ is the deviation of the wave vector $\boldsymbol{K}'$ of diffusely scattered wave in vacuum from the reciprocal lattice point, and $\boldsymbol{K}$ is the incident wave vector.

Expression (3) can be simplified substantially when the approximation of the semi-infinite crystal is valid, i.e. at $\mu_0 t \gg 1$. In such a case, only one quasi-Bloch wave remains in the wave fields of both strong Bragg and diffusely scattered waves, and equation (2) can be reduced to the form

$$R_{DS}(\boldsymbol{k}) = \frac{1}{\gamma_0 S}\left(\frac{CVK^2}{4\pi}\right)^2 F_{dyn} S(\boldsymbol{q})$$

$$S(\boldsymbol{q}) = \langle |\delta\chi_{\boldsymbol{H}+\boldsymbol{q}}|^2\rangle \qquad (4)$$

where V is the crystal volume, the extinction factor $F_{dyn} \approx 1$ describes the modulation of diffuse scattering intensity, which is caused by the extinction of strong Bragg waves, $\delta\chi_{\boldsymbol{H}+\boldsymbol{q}}$ is Fourier component of fluctuating part of the crystal polarizability, $\boldsymbol{q} = \boldsymbol{k} + i\mu_i\boldsymbol{n}$, $\boldsymbol{n}$ is the inner normal to the entrance crystal surface, the interference absorption coefficient can be estimated as $\mu_i \approx (1+b)\mu_0/(2\gamma_0)$ at $|y|, |y'| \gg 1$ and $\mu_i \sim \pi/\Lambda$ at $|y|, |y'| \leqslant 1$, where Λ is the extinction length, and y and y' are the angular deviations of incident and diffusely scattered waves from exact Bragg directions, which are normalized to the width of total reflection range w.

Integrating expression (4) over the Ewald sphere ($K' = K$) near the reciprocal lattice point H, we obtain the 'integral' diffuse component of the reflection coefficient measured by a DCD with widely open detector window:

$$R_{diff}(\Delta\theta) = \int_{K'=K} R_{DS}(\boldsymbol{k})\,\mathrm{d}S_{\boldsymbol{K}'}/K^2 = F_{dyn}(\Delta\theta)\mu^{\delta}_{00}(\Delta\theta)t/\gamma_0 \qquad (5)$$

$$\mu^{\delta}_{00}(\Delta\theta) = \frac{C^2V}{4\lambda^2}\int \mathrm{d}S_{\boldsymbol{K}'}\, S(\boldsymbol{q}) \qquad (6)$$

where $\mathrm{d}S_{K'} = K^2\,\mathrm{d}\Omega_{K'}$ is the element of surface area in the reciprocal space. Performing the two-dimensional integration in (6), we obtain

$$R_{diff}(\Delta\theta) \cong F_{dyn}\frac{\mu_{ds}(\Delta\theta)}{2\gamma_0\mu(\Delta\theta)} \tag{7}$$

$$\mu_{ds}(\Delta\theta) = cC^2E^2m_0J(k_0) \qquad m_0 = \frac{\pi v_c}{4}(H|\chi_{rH}|/\lambda)^2 \tag{8}$$

$$J(k_0) = \begin{cases} b_2\ln\left(\mathrm{e}\dfrac{k_m^2+\mu^2}{k_0^2+\mu^2}\right) + b_3\left(\dfrac{k_0^2}{2k_m^2} - 1\right) \\ \qquad |k_0| \leqslant k_m \\ \left(b_2 - \dfrac{1}{2}b_3\right)\dfrac{k_m^2}{k_0^2} \\ \qquad |k_0| \geqslant k_m \end{cases} \tag{9}$$

$$b_2 = B_1 + \tfrac{1}{2}B_2\cos^2\theta_B \qquad b_3 = \tfrac{1}{2}B_2(\cos^2\theta_B - 2\sin^2\theta_B)$$

$$\mu(\Delta\theta) = \frac{\mu_0}{2\gamma_0}\frac{1+b}{2}\left(1 + \frac{r_i}{|g|}E\right)$$

$$r_1 = \sqrt{\tfrac{1}{2}\left(\sqrt{u^2+v^2} - u\right)} \tag{10}$$

$$u = (z^2 - g^2)E^{-2} + \kappa^2 - 1 \qquad v = 2(zgE^{-2} - p).$$

Here, c is the defect concentration, v_c is the crystal unit cell volume, λ is x-ray wavelength, $k_0 = K\Delta\theta\sin(2\theta_B)$ is the shortest distance from the reciprocal lattice point H to the Ewald sphere, $k_m = 2\pi/ER_{eff}$ defines the boundary between Huang and Stokes–Wilson region, $R_{eff} = R_L\sqrt{Hb}$ for dislocation loops (R_L is the loop radius and b is the modulus of Burgers' vector) and $R_{eff} = \sqrt{H|A_{cl}|}$ for clusters (A_{cl} is the cluster strength). The constants B_1 and B_2 also depend on specific defect characteristics, particularly, for prismatic dislocation loops $B_1 = 4(\pi bR_L^2/v_c)^2/15$ and $B_2 = \beta B_1$, where $\beta = (3\nu^2+6\nu-1)/4(1-\nu)^2$ and ν is the Poisson ratio, whereas for spherical clusters $B_1 = 0$ and $B_2 = (4\pi A_{cl}/v_c)^2$.

In contrast to the known kinematical expressions for the DS intensity integrated over Ewald sphere [3, 4], where the cut-off parameter $k_c = 2\pi/\Lambda$ has been introduced to remove the divergence at $k \to 0$, such a cut-off parameter (μ) having the order of magnitude k_c in the total reflection range has appeared in the expression (9) in a natural way due to the consistent accounting for the dynamical effects in DS. This lifts the restriction on the maximally allowable effective defect radius ($R_{eff} < \Lambda$) and gives the possibility to describe quantitatively in explicit analytical terms the Huang DS intensity also in the total reflection range at both $R_{eff} < \Lambda$ and $R_{eff} \geqslant \Lambda$.

The expression for the diffuse component of the RC R_{diff} (7) includes two factors which describe the characteristic redistribution of diffuse scattering intensity (F_{dyn}) and the extinction gap ($1/\mu$) in the total reflection range.

At sufficiently large angular deviations $|\Delta\theta| \gg w$, where $w = 2C|\chi_{rH}|/(\sqrt{b}\sin 2\theta_B)$ is the width of the total reflection range, one can put $F_{dyn} \cong 1$ and $\mu \cong \mu_0(1+b)/(2\gamma_0)$. Then, for weakly absorbing crystals ($k_c \gg \mu_0$) containing small defects with effective radii $R_{eff} \ll \Lambda$ ($k_m \gg k_c$), the inequalities $|k_0| \gg \mu$ and $k_m \gg \mu$ hold and we obtain, after neglecting μ^2 in (9), the kinematical expression for the diffuse reflectivity:

$$R_{diff}(\Delta\theta) = \frac{\mu_{ds}^{kin}(\Delta\theta)}{(1+b)\mu_0}$$

Figure 1. Lang topograph of the annealed silicon sample (the symmetric 220 reflection of Mo K_{α_1} radiation), magnification 10×.

which almost coincides with the known kinematical one [3, 4] in the symmetric case of Bragg diffraction ($b = 1$) and differs only in terms with b_3 coefficient.

3. Experimental set-up and investigated sample

The measurements of RCs of the investigated sample, which was in the parallel, non-dispersive setting relative to the last reflection of the collimator, were performed using a high-resolution four-circle x-ray DCD. For 111 reflection, the collimator consisted of two separated three-reflection channel-cut perfect Si monochromators in antiparallel setting with symmetric 220 reflections. For 333 reflection, a one-reflection Ge monochromator and a second two-reflection channel-cut Si monochromator in the antiparallel setting were used both with symmetric 333 reflections.

The investigated sample of dislocation-free silicon single crystal (thickness 488 mkm) was cut perpendicularly to the growth axis [111] from a Czochralski-grown ingot with p-type conductivity ($\rho = 10\ \Omega$ cm) and with concentrations of oxygen 1.1×10^{18} cm^{-3} and carbon lower than 1×10^{16} cm^{-3}, respectively. The sample was annealed in air atmosphere at 1080 °C for 6 h.

The transmission x-ray topograph of the sample (symmetric $2\bar{2}0$ reflection of Mo K_{α_1} radiation, figure 1) shows the homogeneous distribution of microdefects with contrast dimensions not exceeding 50 mkm and the concentration estimated to be not less than 1×10^5 cm^{-3}.

4. Treatment of experimental results and discussion

The RC of the sample for 333 reflection of Cu K_{α_1} radiation, which has been measured in the symmetric Bragg diffraction geometry, is shown in figure 2 together with the theoretical RC separately for the central part (total reflection range) and for the tails in logarithmic and double-logarithmic scales. In the fitting procedure, the defect radii and concentrations were the fit parameters. The high sensitivity of the RC to the fit parameters required refining the zeroth position of $\Delta\theta$ scale. To obtain a more accurate fitting in the vicinity of and within the total reflection range, the intrinsic reflection coefficient of the investigated sample

$$R(\Delta\theta) = R_{coh}(\Delta\theta) + R_{diff}(\Delta\theta)$$

(where the coherent (R_{coh}) and diffuse (R_{diff}) components are defined by equations (1) and (7), respectively) was convoluted with the reflection coefficient of the collimator system at the final stage of the fitting procedure.

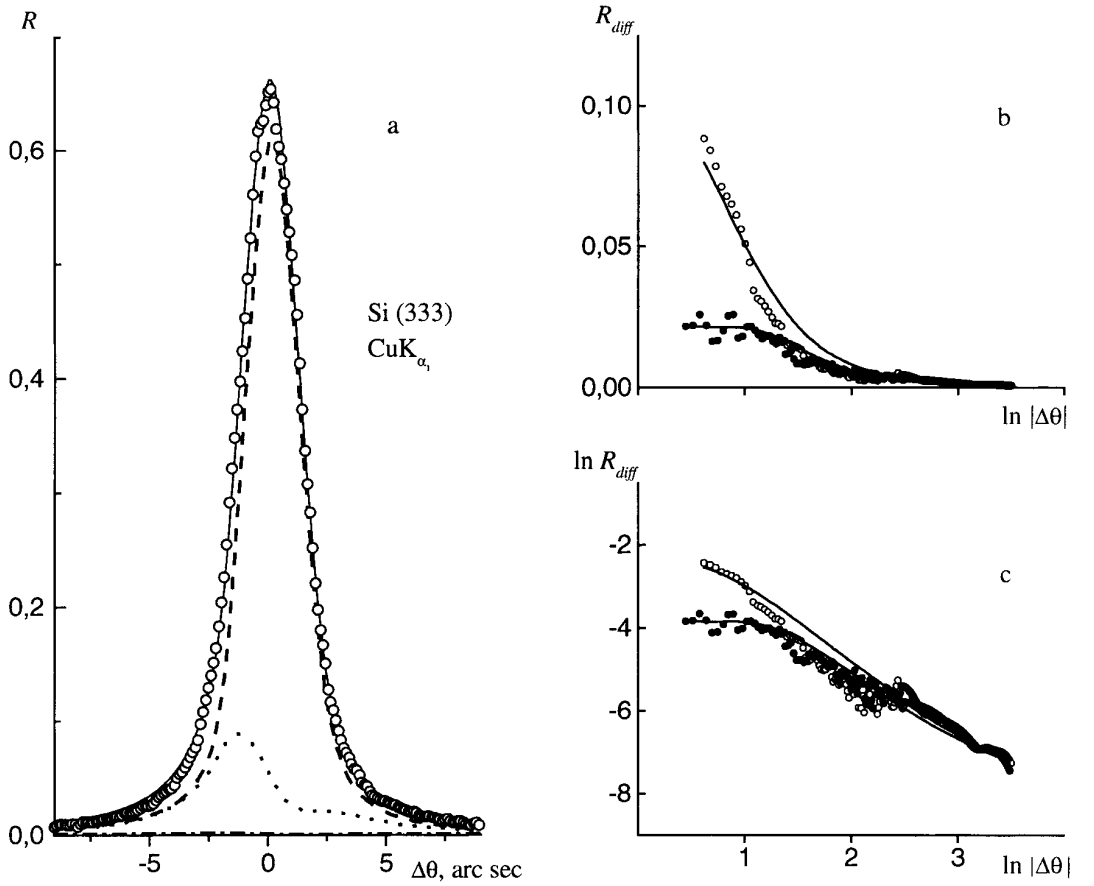

Figure 2. (a) RC of the silicon sample annealed for 6 h at 1080 °C for the symmetric Bragg reflection 333 of Cu K_{α_1} radiation. Full curve is the fitted total RC, dashed and dotted curves are its coherent (R_{coh}) and diffuse (R_{diff}) components, respectively. The diffuse component R_{diff} (b) and ln R_{diff} (c) are plotted versus ln $|\Delta\theta|$, the filled and open circles correspond to $\Delta\theta > 0$ and $\Delta\theta < 0$, respectively, and have been obtained by subtracting R_{coh} from the measured RC.

In the first step of the treatment, the most simplified microdefect models supposing the presence (i.e. the dominant influence on the diffraction pattern) of only spherical clusters (precipitates) or circular dislocation loops were applied to fit the measured RCs for both 111 and 333 reflections. Such attempts, however, failed because it was impossible to simultaneously fit the central part and tails of each RC, on the one hand, and to match the defect parameters for both RCs, on the other hand.

In the second step, we fitted the measured RCs by accounting for the presence of both types of defects (loops and precipitates) simultaneously. The corresponding modification of the formulae (1) and (7)–(10) can be made easily, if the random distribution of defects of both types is supposed to be without mutual correlation. In such a case, ensemble averaging can be performed independently for each defect type, and results in replacing the parameters L_H and μ_{ds} by the corresponding sums of these parameters calculated for each type of defects:

$$L_H = \sum_\alpha L_H^\alpha \qquad \mu_{ds} = \sum_\alpha \mu_{ds}^\alpha$$

where α numerates the defect types.

The exponent L_H of the static Debye–Waller factor for dislocation loops was calculated according to the known expression [5]

$$L_H \cong \frac{1}{2} c_L \frac{R_L^3}{v_c} (Hb)^{3/2}$$

where c_L is the concentration of dislocation loops per unit cell. The formula for L_H in the case of spherical clusters [5] has been modified for the case of disc-shaped precipitates as follows:

$$L_H \cong \begin{cases} c_P n_0 \eta^2/2 & \text{at } \eta^2 \ll 10 \\ c_P n_0 \eta^{3/2} & \text{at } \eta^2 \gg 10 \end{cases}$$

where c_P is the precipitate concentration, $n_0 = \pi R_P^2 h_P / v_c$ is the number of unit cells substituted by the precipitate volume, R_P is the precipitate radius, h_P is the precipitate thickness, $\eta = \alpha_0 n_0^{1/3} H a_0/(2\pi)$, $\alpha_0 = \Gamma\varepsilon(3\pi^2/4)^{1/3}$, $\Gamma = (1+\nu)/3(1-\nu)$, ε is the deformation at precipitate boundary, and a_0 is the lattice constant. The cluster strength has been also modified for the clusters of disc-shaped form as $A_{cl} = \Gamma\varepsilon R_P^2 h_P/2$. In the fitting, the precipitate thickness was assumed to be equal to $h_P = 2R_P/r_a$, and r_a was determined by solving numerically the transcendental equation, which connects the diameter of the disc-shaped precipitate with its thickness [14]. The parameter of the deformation at the amorphous SiO_2 precipitate boundary was put equal to $\varepsilon \approx 0.0242$ [15].

The values of microdefect characteristics determined by fitting the measured RCs for two types of microdefects simultaneously are listed in table 1. As can be seen, the sizes and densities of precipitates and dislocation loops, which have been determined independently for each reflection, are in a good mutual agreement. The densities and sizes of dislocation loops correspond well with the results of x-ray topographic observation (figure 1). It is clear that precipitates with sizes of about 0.6 mkm cannot be resolved by x-ray topograph, but the obtained sizes and densities of precipitates, as well as those of dislocation loops, satisfactorily correlate with known results of direct observations [16–21] and theoretical calculations [20, 21] for silicon single crystals with similar characteristics (initial concentrations of oxygen and carbon, temperature and duration of annealing). It should be remarked here that direct observation methods such as transmission electron microscopy, which are exclusively important for the establishment of the nature (and of some characteristics) of microdefects, are destructive and require a large number of samples to give the representative statistical information about defect sizes and distributions, and cannot provide the full extent of such information from the whole crystal volume as compared to x-ray diffraction methods. Concerning the fit quality of the present x-ray measurement (see figure 2), a good match of the calculated reflectivity with the measured one in the total reflection range and at tails should be noticed, but a worse coincidence is observed in the close vicinity of the Bragg peak. In this region, according to the obtained microdefect radii, lie the boundaries between Huang and Stokes–Wilson scattering regions for both microdefect types. Because of the existence of a spread of actual microdefect radii in the sample, which causes a smearing of these boundaries, better agreement of theory and experiment might be achieved by accounting for the size distributions of microdefects. The correct solution of this problem, however, requires consideration of a realistic model of microdefect size distribution and thorough analysis of all the factors influencing the uniqueness of determined defect characteristics from the view of both diffraction theory and experiment, and this will be investigated separately. On the other hand, it should be emphasized that, in the case when the whole of Huang scattering region even for one type of microdefects lies under Bragg peak, the kinematical approach obviously does not allow one to obtain the unique information about the characteristics of the defects, because then the tails of both diffuse and coherent scattering intensity decrease as $(\Delta\theta)^{-2}$. So, the important advantage of the suggested method is the self-consistent description of coherent and diffuse components of scattering intensity in the whole angular interval including the total reflection range.

In conclusion, the good mutual agreement of the values of defect characteristics determined from the measured RCs for two reflections and the fair correlation of these parameters with the published relevant experimental data can be considered as experimental verification of the developed x-ray characterization method. The results obtained demonstrate its high diagnostic possibilities. In order to fulfil these possibilities, however, it is necessary to use additional experimental and theoretical information about the nature and morphology of defects in the single crystals under investigation.

Table 1. Characteristics of oxygen precipitates ($n_P = c_P/v_c$, R_P, h_P) and dislocation loops ($n_L = c_L/v_c$, R_L) in Czochralski-grown silicon sample annealed at 1080 °C for 6 h.

	hkl	
	111	333
n_P (cm^{-3})	$(5.8 \pm 0.5) \times 10^9$	$(5.4 \pm 0.4) \times 10^9$
R_P (mkm)	0.66 ± 0.06	0.57 ± 0.04
h_P (Å)	135 ± 12	127 ± 9
n_L (cm^{-3})	$(5.9 \pm 0.5) \times 10^5$	$(4.2 \pm 0.3) \times 10^5$
R_L (mkm)	16.6 ± 1.5	16.0 ± 1.1

5. Summary

A theoretical model, based on the generalized dynamical theory of x-ray scattering by imperfect single crystals with randomly distributed defects, has been used to analyse the measured RCs of silicon single crystal containing simultaneously large (dislocation loops) and small (oxygen precipitates) defects. The determined microdefect characteristics are in good agreement for two measured reflections and correlate well with existing experimental and theoretical data. The result obtained allow us to propose a new generalized method of integral DS for the quantitative characterization of various types of microdefects in single crystals, including those with large effective radii.

References

[1] Dederichs P H 1971 *Phys. Rev.* B **4** 1041
[2] Thomas J E, Baldwin T O and Dederichs P H 1971 *Phys. Rev.* B **3** 1167
[3] Larson B C and Young F W Jr 1973 *Z. Naturforsch.* A **28** 626
[4] Larson B C 1975 *J. Appl. Crystallogr.* **8** 150
[5] Krivoglaz M A 1992 *Diffraction of X-Rays and Thermal Neutrons in Imperfect Crystals* (Berlin: Springer)
[6] Patel J R 1975 *J. Appl. Crystallogr.* **8** 186
[7] Holý V and Kubena J 1992 *Phys. Status Solidi* b **170** 9
[8] Bouchard R, Schneider J R, Gupta S, Messoloras S, Stewart R J, Nagasawa H and Zulehner W 1995 *J. Appl. Phys.* **77** 553
[9] Borghesi A, Pivac B, Sassella A and Stella A 1995 *J. Appl. Phys.* **77** 4169
[10] Molodkin V B 1981 *Phys. Metals* **3** 615
[11] Molodkin V B, Olikhovskii S I and Osinovskii M E 1984 *Phys. Metals* **5** 1
[12] Molodkin V B, Olikhovskii S I, Kislovskii E N, Krivitsky V P, Los'A V, Pervak E V, Ice G E and Larson B C 1999 *Met. Phys. Adv. Tech.* **17** 1383
[13] Pinsker Z G 1978 *Dynamical Scattering of X-Rays in Crystals* (Berlin: Springer)
[14] Hu S M 1986 *Appl. Phys. Lett.* **48** 115
[15] Schneider J R, Bouchard R, Graf H A and Nagasawa H 1992 *Acta Crystallogr.* A **48** 804
[16] Patel J R, Jackson K A and Reiss H 1977 *J. Appl. Phys.* **48** 5279
[17] Patel J R 1973 *J. Appl. Phys.* **44** 3903
[18] Murarka S P 1977 *J. Appl. Phys.* **48** 5020
[19] Patrick W, Hearn E, Westdorp W and Bohg A 1979 *J. Appl. Phys.* **50** 7156
[20] Wada K, Inoue N and Kohra K 1980 *J. Cryst. Growth* **49** 749
[21] Livingston F M, Messoloras S, Newman R C, Pike B C, Stewart R J, Binns W J, Brown W P and Wilkes J G 1984 *J. Phys. C: Solid State Phys.* **17** 6253